Decrease of back recombination rate in CdS quantum dots sensitized solar cells using reduced graphene oxide*

Ali Badawi†

Department of Physics, Faculty of Science, Taif University, Taif, Saudi Arabia

(Received 10 September 2014; revised manuscript received 14 November 2014; published online 10 February 2015)

The photovoltaic performance of CdS quantum dots sensitized solar cells (QDSSCs) using the 0.2 wt% of reduced graphene oxide and TiO_2 nanoparticles (RGO+TiO_2 nanocomposite) photoanode is investigated. CdS QDs are adsorbed onto RGO+TiO_2 nanocomposite films by the successive ionic layer adsorption and reaction (SILAR) technique for several cycles. The current density–voltage (J–V) characteristic curves of the assembled QDSSCs are measured at AM1.5 simulated sunlight. The optimal photovoltaic performance for CdS QDSSC was achieved for six SILAR cycles. Solar cells based on the RGO+TiO_2 nanocomposite photoanode achieve a 33% increase in conversion efficiency (η) compared with those based on plain TiO_2 nanoparticle (NP) photoanodes. The electron back recombination rates decrease significantly for CdS QDSSCs based on RGO+TiO_2 nanocomposite photoanodes. The lifetime constant (τ) for CdS QDSSC based on the RGO+TiO_2 nanocomposite photoanode is at least one order of magnitude larger than that based on the bare TiO_2NPs photoanode.

Keywords: reduced graphene oxide, nanocomposite photoanode, back recombination rate, quantum dots sensitized solar cell

PACS: 72.80.Vp, 78.67.Wj, 78.67.Sc, 78.67.Hc **DOI:** 10.1088/1674-1056/24/4/047205

1. Introduction

Recently, semiconductor quantum dots (QDs) have been considered as an alternative to organic dyes molecules in many applications[1,2] QDs possess higher extinction coefficients[3,4] and higher stabilities than metal–organic dyes,[5,6] a large intrinsic dipole moment leading to rapid charge separation,[7,8] and strong absorption.[9] In addition, QDs exhibit attractive characteristics as sensitizers due to their tunable band gaps, by either controlling the size[10] or varying the component concentration.[11] Tuning the band gap for QDs is used to match the solar spectrum.[12,13] Furthermore, QDs have been shown to enable the highly efficient multiple exciton generation (MEG),[2,14] therefore, a single absorbed photon can generate more than one electron–hole pair.[9,15] Several studies were carried out using QDs as photosensitizers.[16–18] Cadmium chalcogenides (CdX: X = Te, Se, S) QDs are suitable sensitizers to check the quantum dots sensitized solar cell (QDSSC) concepts,[19] since their conduction band minimum (CBM) effectively injects electrons to the conduction band (CB) of a wide band gap metal–oxide material such as TiO_2 and ZnO nanoparticles (NPs).[20,21] Furthermore, CdX QDs are direct band gap energy materials and relatively easy to synthesize, thereby tuning their band gaps to harvest much incident energy in the visible region of the solar spectrum.

Two different strategies are mainly used to deposit QDs onto the large band gap metal oxides.[22] One is an *ex situ* strategy, where QDs are first synthesised and then deposited via electrophoretic deposition (EPD),[23] linker-assisted adsorption (LA),[24] or direct adsorption (DA)[25,26] for different dipping times. The other is an *in situ* strategy where QDs grow by either the chemical bath deposition (CBD) technique,[13] or the successive ionic layer adsorption and reaction (SILAR) method.[27] The last method (SILAR) is the one applied in this work, which provides a good surface coverage and produces high-quality nanoparticles (NPs) on a large scale.[28]

Graphene is the thinnest known material in the universe and the strongest ever measured.[29] In the past few years, graphene has become the focus of considerable interest because of its unique electronic properties and other excellent attributes, such as large specific surface area and high transparency.[30,31] Moreover, graphene has an excellent mechanical strength.[32,33] Meanwhile, reduced graphene oxide (RGO) is receiving extensive attention because it possesses similar properties to graphene.[34] For photovoltaic applications, a new type of nanocomposite of low RGO concentrations in TiO_2 NPs (RGO+TiO_2 nanocomposite) is used to improve significantly the electron transportation in a photoelectrode[30,35] and reduce the charge recombination rate. The characteristics of the novel nanocomposite photoanodes can enhance the photovoltaic performance of the assembled solar cells.[34,36] Many studies[34,37] showed that graphene can significantly improve the short circuit current density (J_{sc}) and power conversion efficiency (η) of dye-sensitized solar cells (DSSCs). Fang *et al.*[35] showed that η of DSSC based on graphene oxide/TiO_2 photoelectrodes

*Project supported by the Fund from Taif University, Saudi Arabia (Grant No. 1/435/3524).

†Corresponding author. E-mail: adaraghmeh@yahoo.com

© 2015 Chinese Physical Society and IOP Publishing Ltd

is remarkably higher than that of pure TiO_2. In our previous study,[36] we concluded that QDSSC based on 0.2 weight (wt)% of SWCNTs/TiO_2 nanocomposite photoanode achieves 58% increase in η compared with that based on plain TiO_2 NP photoanodes under an AM1.5 simulated sunlight. Peining *et al.*[38] and Yu *et al.*[39] have shown that 0.2 wt% of CNTs is an optimal concentration in the TiO_2 matrix for the best photovoltaic performance in DSSC.

In this study, we prepared 0.2-wt% RGO+TiO_2 nanocomposite films by mechanical mixing. CdS QDs are used as a sensitizer in QDSSCs. These quantum dots were adsorbed onto RGO+TiO_2 nanocomposite photoanodes using the SILAR technique under ambient conditions. Figure 1 shows an artistic depiction of the basic design of CdS QDSSC based on the RGO+TiO_2 nanocomposite photoanode. Improving the photovoltaic performance of CdS QDSSC using 0.2 wt% of the RGO+TiO_2 nanocomposite photoanode is reported. The effect of the RGO on the photovoltaic parameters (J_{sc}, open circuit voltage (V_{oc}), fill factor (FF), and η) of CdS QDSSCs incorporated by the RGO+TiO_2 nanocomposite photoanode is studied. The electron–hole back recombination rates of CdS QDSSCs are reported by V_{oc} decay measurements. The values of lifetime decay constant (τ) are also calculated.

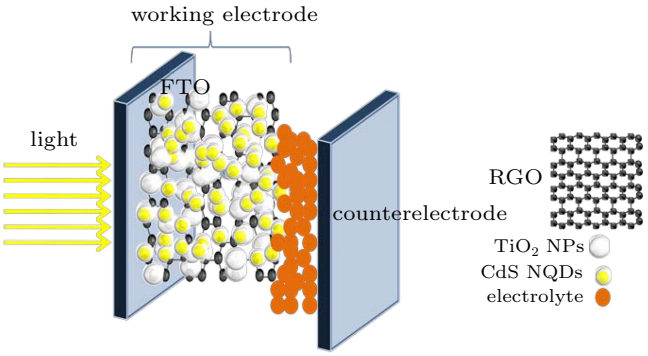


Fig. 1. (color online) An artistic depiction of the basic design of CdS QDSSC based on RGO+TiO_2 nanocomposite photoanode.

2. Experiment

2.1. Preparation of QDSSC electrodes

A colloidal paste of TiO_2 NPs was prepared using the method of Syrrokostas *et al.*[40] as follows: 3 g of commercial Degussa P25 TiO_2 nanopowders (P25) (Degussa AG, Dusseldorf, Germany) was ground in a porcelain pestle and mortar and mixed with 1 ml of distilled water containing acetyl acetone (10% v/v). Acetyl acetone was used as a dispersing agent because it prevents the coagulation of TiO_2 NPs and its influence on the porosity of the film. The paste was diluted further by the slow addition of distilled water (4 ml) under continuous grinding. The addition of water controls the viscosity and final concentration of the paste. Finally, a few drops of a detergent (Triton X-100) were added for reducing the surface tension of the paste, which facilitates even spreading and reducing the formation of surface cracks.

To synthesize 0.2 wt% of RGO+TiO_2 nanocomposite paste, the method of Yu *et al.*[39] was followed. Briefly, RGO (thickness = 0.553.74 nm, size = 0.5 μm–3.0 μm, purity > 99%, purchased from Chengdu Organic Chemicals Co. Ltd.) was rinsed with deionized water three times and dried at 60 °C under ambient conditions. Then 6 mg of RGO was added to the previous TiO_2 NPs paste and dispersed using an ultrasonic horn for 30 min. After stirring for 2 h, using the doctor blade technique, the 0.2 wt% RGO+TiO_2 nanocomposite paste was coated on a transparent conducting glass substrate made from SnO_2:F (FTO) (purchased from Solaronix, TCO22-7 sheet resistance = 7 Ω/sq and > 80% transmittance in the visible region). Then, the films were sintered at 450 °C for 1 h. After cooling to room temperature, CdS QDs were deposited on the RGO+TiO_2 nanocomposite photoanode layer by the SILAR deposition method. Two separated solutions of 0.5-M $Cd(NO_3)_2$ in ethanol and 0.5-M Na_2S in methanol were prepared. The RGO+TiO_2 nanocomposite photoanodes were dipped into 0.5-M $Cd(NO_3)_2$ solution for 30 s and rinsed with ethanol and then, dipped into 0.5-M Na_2S for 30 s and rinsed again with methanol. The two-step dipping procedure was considered to be one cycle. This sequential coating was repeated for several cycles to form seven working photoanodes marked from a to g. After solvent evaporation, the final nanocomposite film thickness was 8 ± 1 μm. The photoanodes were then kept at room temperature. The counter electrodes were FTO substrate sheets coated with Pt.

2.2. Assembly of CdS QDSSC

The working photoanode and Pt counter electrode were assembled into a sandwich-type cell using clamps. Both electrodes were sealed using a hot-melt polymer sheet (Solaronix, SX1170-25PF) that was 25-μm thick to avoid the evaporation of the electrolyte. The active area of the assembled cells was 1 cm × 1 cm. Finally, an iodide electrolyte solution was prepared by dissolving 0.127 g of 0.05-M iodine (I_2) in 10 ml of water-free ethylene glycol and then adding 0.83 g of 0.5-M potassium iodide (KI). The electrolyte was inserted into the cell with a syringe, filling the space between the two electrodes.

2.3. Measurements

The absorption spectra of the working photoanodes were recorded using an ultraviolet-visible (UV-Vis) spectrophotometer (JASCO V-670). The current density–voltage (J–V) characteristics were recorded with a Keithley 2400 voltage source/ammeter using Green Mountain IV-Sat 3.1 software, while the CdS QDSSCs were subjected to a solar simulator

(ABET technologies, Sun 2000 Solar Simulators, USA) operating at 100 mW/cm^2 (AM1.5). The intensity of the incident solar illumination was adjusted to 1 sun condition using a Leybold certified silicon reference solar cell (Model: (57863) Solar cell 2 V/0.3 A STE 4/100). The photo-voltage decay rates of the assembled CdS QDSSCs were measured using a Tektronix 500 MHz oscilloscope. All experiments were carried out under ambient conditions.

3. Results and discussion

3.1. Characterization of CdS QDs sensitized RGO + TiO_2 nanocomposite photoanodes (the working photoanodes)

The UV-Vis absorption spectra of CdS QDs sensitized RGO+TiO_2 nanocomposite photoanodes for several SILAR deposition cycles (0, 2, 3, 4, 6, and 8) are shown in Fig. 2. It is clearly seen that the absorption is enhanced as the number of SILAR cycles increases, due to a greater amount of CdS QD loading. Furthermore, the absorption edges of CdS QDs sensitized (RGO+TiO_2) nanocomposite photoanodes are red-shifted as the number of SILAR cycles increases also. The red-shifts of the absorption shoulder and onset position with increasing SILAR cycles imply a slight growth of the CdS QDs. Such red shifts are in reasonable agreement with the results in Refs. [18] and [41].

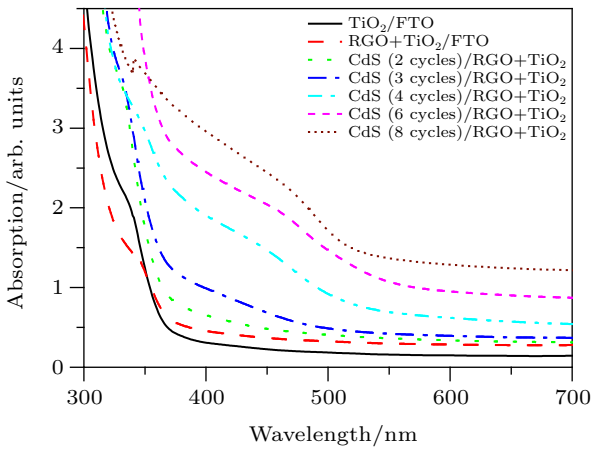


Fig. 2. (color online) UV-Vis absorption spectra of CdS QDs sensitized RGO+TiO_2 nanocomposite photoanodes for different SILAR deposition cycles.

Figure 3 shows the UV-Vis absorption spectra of a plain TiO_2 NPs photoanode, a RGO+TiO_2 nanocomposite photoanode, a CdS QDs (6 cycles) sensitized plain TiO_2 NPs photoanode, and a CdS QDs (6 cycles) sensitized RGO+TiO_2 nanocomposite photoanode. It is clearly evident that the absorption of the CdS QDs (six cycles) sensitized RGO+TiO_2 nanocomposite photoanode is higher than that of the CdS QDs (6 cycles) sensitized plain TiO_2 NPs photoanode. This behavior indicates that more CdS QDs have been adsorbed on the RGO+TiO_2 nanocomposite photoanode. Such an increase of CdS QDs in quantity is due to the high roughness and porosity of the RGO+TiO_2 nanocomposite surface.[35,42]

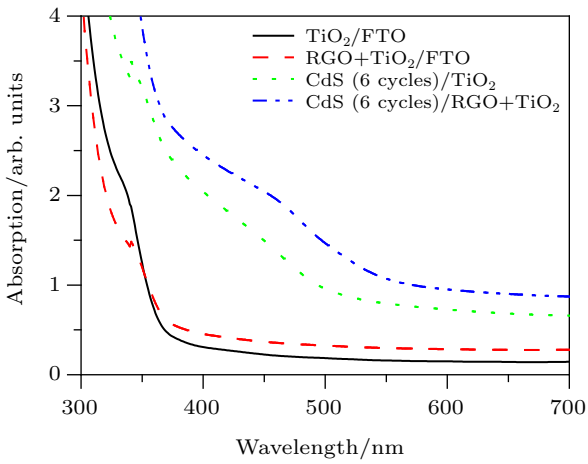


Fig. 3. (color online) UV-Vis absorption spectra of the plain TiO_2 photoanode, RGO+TiO_2 nanocomposite photoanode, CdS QDs (six cycles) sensitized TiO_2 NPs photoanode, and CdS QDs (six cycles) sensitized RGO+TiO_2 nanocomposite photoanode.

3.2. Photovoltaic performance of CdS QDSSCs using RGO + TiO_2 nanocomposite photoanode

The photovoltaic performance of CdS QDSSCs based on RGO+TiO_2 nanocomposite photoanodes for several SILAR deposition cycles is investigated. Figure 4 shows the *J*–*V* characteristic curves which are measured under a simulated sunlight with an intensity of 100 mW/cm^2 (AM1.5). The photovoltaic characteristic parameters (V_{oc}, J_{sc}, FF, and η) for CdS QDSSCs are given in Table 1. Up to six SILAR cycles, it is clearly observed that both J_{sc} and η increase, peaking at 1.83 mA/cm^2 and 0.37% respectively. These values lower again to 1.31 mA/cm^2 and 0.26% for seven SILAR cycles and to 0.92 mA/cm^2 and 0.17% for eight SILAR cycles. These results could be explained in terms of, as the number of SILAR cycles increases up to six cycles, an additional quantity of CdS QDs are loaded because of the high roughness and porous surface of the RGO+TiO_2 nanocomposite[35,42] which, in turn, leads to increasing the absorption of the incident solar power (as shown in Fig. 2). Moreover, increasing the number of SILAR cycles causes a significant red shift of the absorption shoulder (as also shown in Fig. 2) and thus causes the relatively high absorption of the incident photons from the visible solar spectrum. While, as the number of SILAR cycles increases to more than six cycles, the extra quantity of CdS QDs leads to blocking the nanopores of the RGO+TiO_2 nanocomposite layer, causing both J_{sc} and η to decrease. These results are in good agreement with our previous studies.[10,43] We have made measurements on J_{sc} and η of CdSe QDs-sensitized TiO_2 NPs using the DA technique. We find the values of J_{sc} and η for the 6-h dipping time are better than those of higher dipping times.

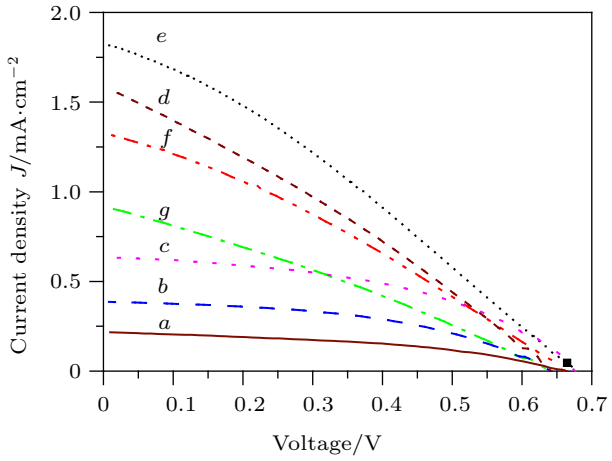


Fig. 4. (color online) *J–V* characteristics curves of CdS QDSSCs using RGO+TiO_2 nanocomposite photoanode for several SILAR cycles (curve *a* to curve *g* refers to two to eight cycles).

Table 1. *J–V* characteristic parameters of CdS QDSSCs using RGO+TiO_2 nanocomposite photoanode for several SILAR cycles (curve *a* to curve *g* refers to two to eight cycles).

No. of SILAR cycles	V_{oc}/V ±0.01	J_{sc}/(mA/cm^2) ±0.01	*FF*	η/(±0.01)%
2	0.65	0.22	0.34	0.07
3	0.66	0.39	0.34	0.10
4	0.67	0.63	0.33	0.16
5	0.65	1.58	0.30	0.29
6	0.66	1.83	0.30	0.37
7	0.66	1.31	0.28	0.26
8	0.66	0.92	0.27	0.17

Figure 5 shows the *J–V* characteristic curves of CdS QDSSCs based on both the plain TiO_2NP photoanode and the RGO+TiO_2 nanocomposite photoanode for six-SILAR deposition cycles. The photovoltaic parameters for both QDSSCs are summarized in Table 2. It is clearly observed that there are notable increases in V_{oc} ($\sim$ 10%), J_{sc} ($\sim$ 26%), and η ($\sim$ 33%) in CdS QDSSCs based on the RGO+TiO_2 nanocomposite as compared with those based on plain TiO_2 NPs under an AM1.5 simulated sunlight. These considerable improvements in the photovoltaic parameters for CdS QDSSCs based on the RGO+TiO_2 nanocomposite photoanode are mainly attributed to many factors. First, the enhancement in the absorption of the RGO+TiO_2 nanocomposite photoanode, due to the rough surface structure of RGO+TiO_2 nanocomosite film,[42] which leads to increasing the CdS QD loading on the film. Second, the rapid electron transport through RGO, offering fast interpaths due to the superior electrical conductivity of RGO ($\sim 4 \times 10^3$ $\Omega^{-1}\cdot m^{-1}$ [44]) compared with that of the TiO_2 NPs ($\sim 8.11 \times 10^{-9}$ $\Omega^{-1}\cdot m^{-1}$ [45]). The addition of a small amount of RGO leads to improving the electron mobility of the nanocomposite.[38,39,42] The RGO dispersed into the TiO_2 matrix facilitates the faster transport of photoexcited electrons (from the CdS QDs) across the TiO_2 network and the collection at the FTO surface. Our results are in good agreement with the results in Refs. [38] and [39]. Peining *et al.*[38] fabricated DSSCs using TiO_2 coated with CNTs (TiO_2-CNTs). In their work, they concluded that the TiO_2-CNT content (0.2 wt%) cell showed a $\sim$ 50% increase in η. They attributed this enhancement mainly to the improvement in interconnectivity between TiO_2 particles and TiO_2-CNTs in the porous TiO_2 film. Third, the electron back recombination rate decreases due to the existence of RGO in the nanocomposite photoanode, as discussed below.

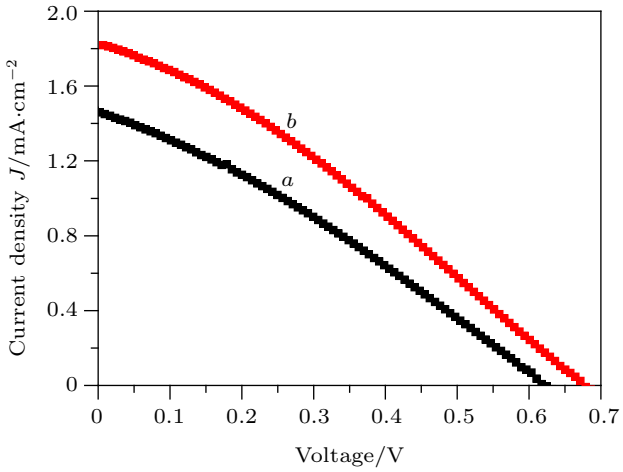


Fig. 5. (color online) *J–V* characteristic curves of CdS QDSSCs using (curve *a*) plain TiO_2NPs photoanode and (curve *b*) RGO+TiO_2 nanocomposite photoanode for six SILAR cycles.

Table 2. *J–V* characteristic parameters of CdS QDSSCs with and without RGO working electrode for six SILAR cycles.

Working electrode	V_{oc}/V ±0.01	J_{sc}/(mA/cm^2) ±0.01	*FF*	η/(±0.01)%
Without RGO	0.61	1.45	0.31	0.28
With RGO	0.66	1.83	0.30	0.37

Figure 6(a) shows V_{oc} decay rates of CdS QDSSCs based on both plain TiO_2NPs and RGO+TiO_2 nanocomposite photoanodes for six SILAR cycles, measured by using a 500-MHz oscilloscope (Tektronix). It is clearly seen that the V_{oc} decay rate of CdS QDSSCs based on the RGO+TiO_2 nanocomposite photoanode is much slower than that when using the plain TiO_2NPs photoanode. This deliberated decay implies that the charge recombination between the injected electrons and the holes is remarkably retarded. RGO facilitates the electron transport from CdS QDs across the TiO_2 network to the FTO surface, since the RGO energy level lies between the CB of TiO_2 and FTO. The energy level diagram of CdS QDSSC using the RGO+TiO_2 photoanode is shown in Fig. 6(b). The stepwise energy levels of CdS QDs, TiO_2, RGO, and FTO are beneficial for electrons to transport from the conduction band of CdS QDs to the FTO substrate. RGO leads to reducing the electron back recombination rate significantly. There-

fore, RGO enhances the photovoltaic performance of CdS QDSSCs.

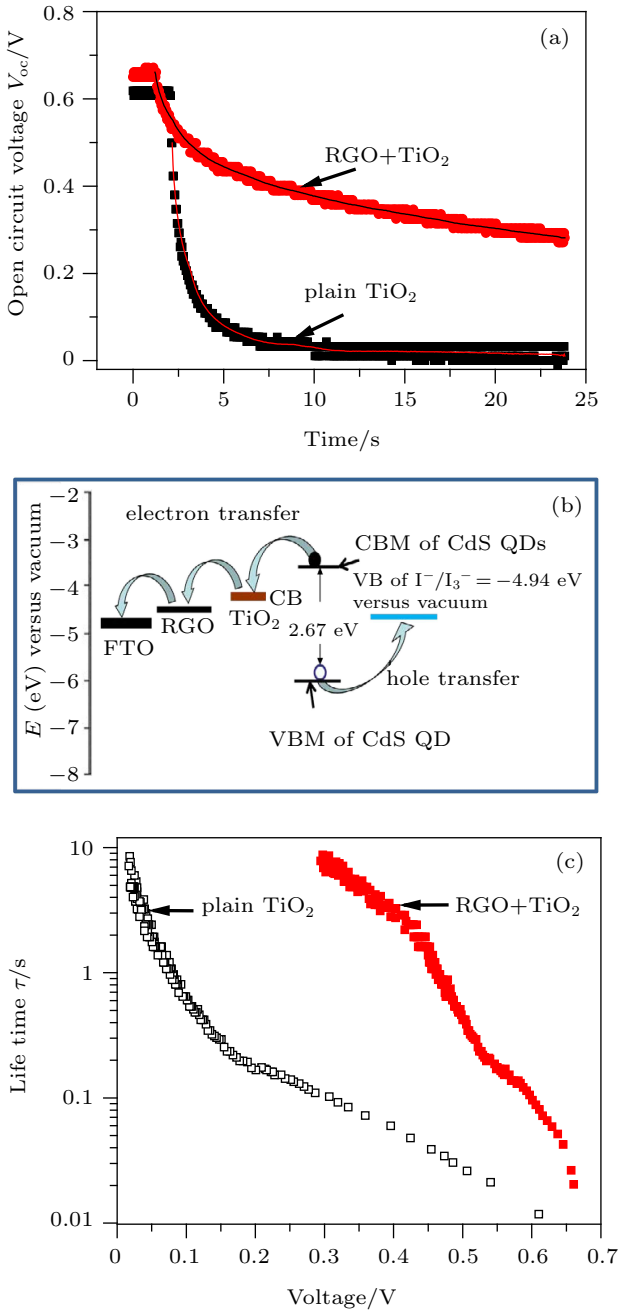


Fig. 6. (color online) (a) Open circuit voltage (V_{oc}) decay rates of CdS QDSSCs based on both plains. The TiO_2NPs photoanode and RGO+TiO_2 nanocomposite photoanode, (b) the energy level diagram of CdS QDSSC using the RGO+TiO_2 photoanode, where the Fermi levels of TiO_2, RGO, and redox (I^-/I_3^-) are set to be at −4.21,[48] −4.42,[48] and −4.94 eV.[49] respectively, and (c) the variations of electron lifetime τ with voltage, obtained from Eq. (1) for six SILAR cycles

The electron lifetime constant (τ) as a function of the decaying V_{oc} is calculated from the following equation:[46,47]

$$\tau = -\frac{k_B}{e}\left(\frac{dV_{oc}}{dt}\right)^{-1}. \quad (1)$$

The values of lifetime constant (τ) of CdS QDSSCs based on both plain TiO_2NPs and RGO+TiO_2 nanocomposite photoanodes for six SILAR cycles are shown in Fig. 6(c). It is clearly seen that τ for CdS QDSSCs based on the RGO+TiO_2 nanocomposite photoanode is at least one order of magnitude larger than that based on the plain TiO_2NPs photoanode. This novel evidence verifies that RGO acts as a blocking layer to reduce the back electron recombination in QDSSCs. Similar results were achieved in Refs. [46] and [47]. Al-juaid *et al.*[46] concluded that the addition of a blocking layer of ZnO to DSSCs plays an important role in reducing the back electron–carrier recombination, which enhances the whole efficiency of DSSCs. In our work, RGO facilitates the electrons transport from CdS QDs across the TiO_2 network to the FTO surface as mentioned before, while the blocking ZnO layer[46] prevents electrons from recombining due to the energy barrier caused by the ZnO layer.

4. Conclusions

We synthesize a nanocomposite paste of 0.2 wt% of reduced graphene oxide (RGO) and TiO_2 nanoparticles (NPs) (RGO+TiO_2 nanocomposite) to construct working photoanodes for quantum dots sensitized solar cells (QDSSCs). CdS QDs as a sensitizer for QDSSCs are adsorbed onto RGO+TiO_2 nanocomposite films by a successive ionic layer adsorption and reaction (SILAR) technique. For six SILAR cycles, a considerable enhancement (∼ 33%) in the energy conversion efficiency (η) is achieved in CdS QDSSCs based on RGO+TiO_2 nanocomposite as compared with other results based on plain TiO_2 NPs under AM1.5 simulated sunlight. The open circuit voltage (V_{oc}) decay rate of CdS QDSSCs based on the RGO+TiO_2 nanocomposite photoanode is much slower than that using the plain TiO_2NPs photoanode. This evidence indicates that electron back recombination rates decrease significantly due to the existence of RGO in the nanocomposite photoanodes. The lifetime constant (τ) for CdS QDSSCs based on the RGO+TiO_2 nanocomposite photoanode is at least one order of magnitude larger than that based on the bare TiO_2NPs photoanode.

Acknowledgment

We wish to thank the Quantum Optics Group at Taif University for their assistance during this work. Also, I sincerely acknowledge the helpful and useful discussion with professor Hassan Talaat (physics professor) at the University of Ain Shams.

References

[1] Badawi A, Al-Hosiny N, Abdallah S, Negm S and Talaat H 2013 *Sol. Energy* **88** 137
[2] Samadpour M, Zad A I and Molaei M 2014 *Chin. Phys. B* **23** 047302
[3] Yang Z and Chang H T 2010 *Sol. Energy Mater. Sol. Cells* **94** 2046
[4] Lin M C and Lee M W 2011 *Elec. Comm.* **13** 1376
[5] Li Y, Pang A, Zheng X and Wei M 2011 *Electrochim. Acta* **56** 4902
[6] Yum J H, Choi S H, Kim S S, Kim D Y and Sung Y E 2007 *J. Korean Phys. Soc.* **10** 257

[7] Prabakar K, Seo H, Son M and Kim H 2009 *Mater. Chem. Phys.* **117** 26
[8] Emin S, Singh S P, Han L, Satoh N and Islam A 2011 *Sol. Energy* **85** 1264
[9] Tubtimtae A, Wu K L, Tung H Y, Lee M W and Wang G J 2010 *Elec. Comm.* **12** 1158
[10] Badawi A, Al-Hosiny N, Abdallah S and Talaat H 2013 *Materials Science-Poland* **31** 6
[11] Al-Hosiny N, Abdallah S, Badawi A, Easawi K and Talaat H 2014 *Mater. Sci. Semicond. Process.* **26** 238
[12] Kamat P V 2007 *J. Phys. Chem. C* **111** 2834
[13] Xie Y, Yoo S H, Chen C and Cho S O 2012 *Mater. Sci. Eng. B* **177** 106
[14] Ma W, Zhang F and Meng S 2014 *Chin. Phys. B* **23** 086801
[15] Fan S Q, Kim D, Kim J J, Jung D W, Kang S O and Ko J 2009 *Elec. Comm.* **11** 1337
[16] Jiao J, Zhou Z J, Zhou W H and Wu S X 2013 *Mater. Sci. Semicond. Process.* **16** 435
[17] Kamat P V 2008 *J. Phys. Chem. C* **112** 18737
[18] Wang X, Zheng J, Sui X, Xie H, Liu B and Zhao X 2013 *Dalton Transactions* **42** 14726
[19] Mora Seró I a, SixtoGiménez, Moehl T, Fabregat Santiago F, Lana Villareal T, Gómez R and Bisquert J 2008 *Nanotechnology* **19** 424007
[20] Xiang B T, Zhou B X, Bai J, Zheng Q, Liu Y B, Cai W M and Cai J 2008 *Chin. Phys. B* **17** 3713
[21] Khurana G, Sahoo S, Barik S K and Katiyar R S 2013 *J. Alloys Compd.* **578** 257
[22] Ruhle S, Shalom M and Zaban A 2010 *Chem. Phys. Chem.* **11** 2290
[23] Salant A, Shalom M, Hod I, Faust A, Zaban A and Banin U 2010 *ACS Nano* **4** 5962
[24] Bang J H and Kamat P V 2009 *ACS Nano* **3** 1467
[25] Pernik D R, Tvrdy K, Radich J G and Kamat P V 2011 *J. Phys. Chem. C* **115** 13511
[26] Badawi A, Easawi K, Al-Hosiny N and Abdallah S 2014 *Mater. Sci. Appl.* **5** 27
[27] Kongkanand A, Tvrdy K, Takechi K, Kuno M and Kamat P V 2008 *J. Am. Chem. Soc.* **130** 4007
[28] Hu Y, Wang B, Zhang J, Wang T, Liu R, Zhang J, Wang X and Wang H 2013 *Nanoscale Research Letters* **8** 222
[29] Ding J, Wang M, Deng J, Gao W, Yang Z, Ran C and Zhang X 2014 *J. Alloys Compd.* **582** 29
[30] Li B, Liu T, Wang Y and Wang Z 2012 *J. Colloid Interf. Sci.* **377** 114
[31] Li P J, Chen K, Chen Y F, Wang Z G, Hao X, Liu J B, He J R and Zhang W L 2012 *Chin. Phys. B* **21** 118101
[32] Yan J, Uddin M J, Dickens T J and Okoli O I 2013 *Sol. Energy* **96** 239
[33] Anwar H, George A E and Hill I G 2013 *Sol. Energy* **88** 129
[34] Song J, Yin Z, Yang Z, Amaladass P, Wu S, Ye J, Zhao Y, Deng W Q, Zhang H and Liu X W 2011 *Chemistry: A European Journal* **17** 10832
[35] Fang X, Li M, Guo K, Zhu Y, Hu Z, Liu X, Chen B and Zhao X 2012 *Electrochimica Acta* **65** 174
[36] Badawi A, Al-Hosiny N, Abdallah S, Merazga A and Talaat H 2014 *Mater. Sci. Semicond. Process.* **26** 162
[37] Luan X, Chen L, Zhang J, Qu G, Flake J C and Wang Y 2013 *Electrochimica Acta* **111** 216
[38] Peining Z, Nair A S, Shengyuan Y, Shengjie P, Elumalai N K and Ramakrishna S 2012 *J. Photochem. Photobio. A: Chemistry* **231** 9
[39] Yu J, Fan J and Cheng B 2011 *J. Power Sources* **196** 7891
[40] Syrrokostas G, Giannouli M and Yianoulis P 2009 *Renewable Energy* **34** 1759
[41] Zhang Y, Zhu J, Yu X, Wei J, Hu L and Dai S 2012 *Sol. Energy* **86** 964
[42] Lee E S, Lee K M, Yoon S I, Ko Y G and Shin D H 2013 *Curr. Appl. Phys.* **13**, Suppl. 2 S26-S29
[43] Abdallah S, Al-Hosiny N and Badawi A 2012 *J. Nanomater.* **2012** 6
[44] Ma P C, Siddiqui N A, Marom G and Kim J K 2010 *Composites: Part A* **41** 1345
[45] Pomoni K, Sofianou M V, Georgakopoulos T, Boukos N and Trapalis C 2013 *J. Alloys Compd.* **548** 194
[46] Al-Juaid F, Merazga A, Al-Baradi A and Abdel-wahab F 2013 *Solid State Electron.* **87** 98
[47] Kim J, Choi H, Nahm C, Moon J, Kim C, Nam S, Jung D R and Park B 2011 *J. Power Sources* **196** 10526
[48] Kim D Y, Joshi B N, Park J J, Lee J G, Cha Y H, Seong T Y, In Noh S, Ahn H J, Al-Deyabe S S and Yoon S S 2014 *Ceramics International* **40** 11089
[49] Yu P, Zhu K, Norman A G, Ferrere S, Frank A J and Nozik A J 2006 *J. Phys. Chem. B* **110** 25451